http://dx.doi.org/10.5012/bkcs.2013.34.6.1679

# Effect of Partial Substitution of Magnetic Rare Earths for La on the Structure, Electric Transport And Magnetic Properties of Oxygen Deficient Phase $LaSr_2MnCrO_{7-\delta}$

**Devinder Singh,* Sushma Sharma, Arun Mahajan, Suram Singh, and Rajinder Singh**

*Department of Chemistry, University of Jammu, Jammu-180 006, India. *E-mail: drdssambyal@rediffmail.com*
*Received January 29, 2013, Accepted March 11, 2013*

Intergrowth perovskite type complex oxides $La_{0.8}Ln_{0.2}Sr_2MnCrO_{7-\delta}$ (Ln=La, Nd, Gd, and Dy) have been synthesized by sol-gel method. Rietveld profile analysis shows that the phases crystallize with tetragonal unit cell in the space group *I4/mmm*. The unit cell parameters *a* and *c* decrease with decreasing effective ionic radius of the lanthanide ion. The magnetic studies suggest that the ferromagnetic interactions are dominant due to $Mn^{3+}$–O–$Mn^{4+}$ and $Mn^{3+}$–O–$Cr^{3+}$ double exchange interactions. Both Weiss constant (θ) and Curie temperature ($T_C$) increase with decreasing ionic radius of lanthanide ion. It was found that the transport mechanism is dominated by Mott's variable range hopping (VRH) model with an increase of Mott localization energy.

**Key Words :** Sol-gel method, Rietveld refinement, Double-exchange interaction, Mott's variable range hopping model

## Introduction

Layered mixed valence manganites (La, Sr)$_3Mn_2O_7$ of Ruddlesden-Popper phases ($n$ = 2) have been in the focus of research efforts for the last two decades due to their ability to exhibit a wide variety of interesting functional properties, such as the colossal magnetoresistance effect, the tunneling magnetoresistance and fascinating magnetic properties.[1-3] In this system, two ferromagnetic $MnO_2$ layers are separated by a rock-salt-type block layer (La, Sr)$_2O_2$, keeping the quasi-two-dimensional networks of the $MnO_6$ octahedra. The perovskites (La, Sr)$MnO_3$ and layered perovskites (La, Sr)$_3Mn_2O_7$ are the $n = \infty$ and $n$ = 2 members of the series of Ruddlesden-Popper (RP) phases $A_{n+1}B_nO_{3n+1}$, respectively. The layered structure, and the corresponding two-dimensional Mn–O–Mn network of the layered perovskites make them show some interesting properties different from the well known perovskites. In the particular context of the manganites the mixed valency ($Mn^{3+}$/$Mn^{4+}$) leads to strong ferromagnetic (FM) interactions arising from the $Mn^{3+}$–O–$Mn^{4+}$ bonds due to double-exchange (DE) mechanism.[4,5] In addition to DE interactions the lattice distortion is also believed to play an important role through strong electron–phonon coupling which arises from the Jahn-Teller (JT) distortion around the $Mn^{3+}$ ions.[6,7]

During the past several years, there have been increasing reports on the effects of Mn-site element substitution. Among these doping elements, Cr-doping at Mn site in manganites has attracted more attention because Cr-doping has a spectacular effect.[8-10] However, very few reports have appeared on the effect of Cr-doping at Mn site for bilayered perovskite manganites. Recently, the effect of Cr-doping on charged-ordered (CO) state of the bilayered manganite $LaSr_2Mn_2O_7$ is investigated through the measurement of electrical transport and magnetic properties.[11-13] Since the properties of perovskite oxides are strongly affected by chemical factors, such as the average cationic radius $\langle r_A \rangle$ in the A-site[14-16] and the A-site cationic size mismatch,[17,18] it was thought interesting to make partial substitution at La site by other rare-earth ions in chromium substituted manganites. In view of this, bilayered manganites of composition $La_{0.8}Ln_{0.2}Sr_2MnCrO_7$ (Ln=La, Nd, Gd, and Dy) have been synthesized by sol-gel method. Their crystal structure has been determined by Rietveld analysis of the X-ray diffraction data. The electrical transport and magnetic properties have been investigated as a function of temperature.

## Experimental

The polycrystalline samples $La_{0.8}Ln_{0.2}Sr_2MnCrO_7$ (Ln=La, Nd, Gd, and Dy) were synthesized by standard sol-gel technique. 99.9% pure chemicals of $La_2O_3$, $Nd_2O_3$, $Gd_2O_3$, $Dy_2O_3$, $SrCO_3$, $Cr(NO_3)_3{\cdot}9H_2O$, and $Mn(CH_3COO)_2{\cdot}4H_2O$ were used as starting materials. Prior to use, $La_2O_3$, $Nd_2O_3$, $Gd_2O_3$, and $Dy_2O_3$ were calcined at 1000 °C for 10 h in air to remove any hydrogeno-carbonate impurities. Stoichiometric amounts of $La_2O_3$, $Nd_2O_3$, $Gd_2O_3$, $Dy_2O_3$, $SrCO_3$, $Cr(NO_3)_3{\cdot}9H_2O$, and $Mn(CH_3COO)_2{\cdot}4H_2O$ were dissolved in a minimum quantity, typically 150 mL, of a 1:1 solution of analar 6 M nitric acid and distilled water. The mixed solutions were thoroughly stirred using magnetic stirrers for about 2 h and then citric acid was added with a molar ratio of citric acid to total metal ions being set at 3:1. The pH of each solution was adjusted to neutral value using the aqueous $NH_3$ solution to avoid precipitation. The solutions were then slowly evaporated at 95 °C on a hot plate to get gel. The gels were further dried at 300 °C until each self-ignited and burnt into soft black powder. The black precursor powders were then ground and heated at 650 °C for 3 h. During this process a number of gases, *viz*. CO, $CO_2$, organic products, water vapors, *etc*. evolve as a result of decomposition of mainly citrates. The resulting powders were micro-milled and press-

ed into pellets at a pressure of 20 MPa and then calcined at 1280 °C for 40 h with a number of intermediate grindings and pelletizings. Finally, the samples were cooled down slowly to room temperature in the furnace.

Room temperature X-ray diffraction data of the phases were recorded with Bruker AXS diffractometer type D 76181 (Karlsruhe, Germany) using $CuK_\alpha$ radiations in the 2θ range 20-80°. Rietveld refinements of the crystal structure were performed using GSAS program.[19] The line shape of the diffraction peaks was generated by a pseudo-Voigt function. The background was chosen by interpolation between selected points in regions devoid of Bragg reflections.

The electrical resistivity of the sintered pellets of the phases was recorded by four probe method in the temperature range 150-350 K. Thin copper wires were attached to the surface of pellet for the purpose of electrodes with silver epoxy. The densities of the sintered pellets were determined by Archimedes method. The magnetic susceptibility of the polycrystalline phases was measured by Faraday technique in the temperature range 100-300 K using $Hg[Co(SCN)_4]$ as calibrant. All magnetic susceptibility values were corrected for diamagnetism of the constituent ions.

## Results and Discussion

XRD patterns for all the samples of $La_{0.8}Ln_{0.2}Sr_2MnCrO_7$ (Ln = La, Nd, Gd, and Dy) are presented in Figure 1. All diffraction peaks were indexed using $Sr_3Ti_2O_7$-type tetragonal structure in the space group *I4/mmm*, indicating a single phase of bilayer structure. The Rietveld refinements were carried out in the space group *I4/mmm* starting with

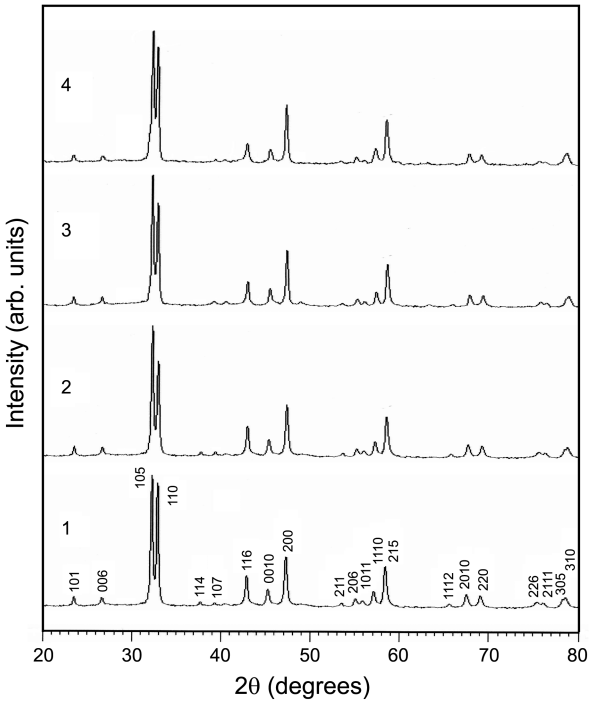


**Figure 1.** X-ray powder diffraction patterns of $LaSr_2MnCrO_7$(1), $La_{0.8}Nd_{0.2}Sr_2MnCrO_7$ (2), $La_{0.8}Gd_{0.2}Sr_2MnCrO_7$ (3), and $La_{0.8}Dy_{0.2}Sr_2MnCrO_7$ (4).

**Table 1.** Structural parameters obtained from the Rietveld refinement of X-ray diffraction pattern for samples $La_{0.8}Ln_{0.2}Sr_2MnCrO_7$. The atomic sites are: Ln/Sr(1) 2b[0, 0, 0.5]; Ln/Sr(2) 4e[0, 0, *z*]; Mn/Cr 4e[0, 0, *z*]; O(1) 2a[0, 0, 0]; O(2) 4e[0, 0, *z*]; O(3) 8g[0, 0.5, *z*] in the space group *I4/mmm*

| Ln | | La | Nd | Gd | Dy |
|---|---|---|---|---|---|
| *a* (Å) | | 3.8486(1) | 3.8454(1) | 3.8434(1) | 3.8418(1) |
| *c* (Å) | | 20.0709(3) | 20.0191(7) | 19.9596(9) | 19.9216(8) |
| *V* (Å$^3$) | | 297.28(6) | 296.02(4) | 294.84(4) | 294.03(7) |
| *z* | Ln/Sr(2) | 0.3143(2) | 0.3156(1) | 0.3141(2) | 0.3119(3) |
| | Mn/Cr | 0.0967(5) | 0.0984(3) | 0.0987(4) | 0.0968(8) |
| | O(2) | 0.2065(2) | 0.2003(7) | 0.2009(8) | 0.1937(9) |
| | O(3) | 0.0891(2) | 0.0917(6) | 0.0919(9) | 0.0892(9) |
| $U_{iso}$ (Å$^2$) | Ln/Sr(1) | 0.0168(4) | 0.0189(4) | 0.0209(3) | 0.0197(4) |
| | Ln/Sr(2) | 0.0208(6) | 0.0251(5) | 0.0235(5) | 0.0239(6) |
| | Mn/Cr | 0.0258(9) | 0.0308(7) | 0.0273(2) | 0.0262(2) |
| | O(1) | 0.0313(5) | 0.0408(1) | 0.0610(2) | 0.0690(7) |
| | O(2) | 0.0594(9) | 0.0471(2) | 0.0447(9) | 0.0461(3) |
| | O(3) | 0.0615(3) | 0.0535(4) | 0.0471(7) | 0.0536(4) |
| Occupancy | O(1) | 0.962(4) | 0.959(4) | 0.956(5) | 0.960(4) |
| | O(2) | 1 | 1 | 1 | 1 |
| | O(3) | 1 | 1 | 1 | 1 |
| $R_{wp}$ | | 0.0813 | 0.0551 | 0.0753 | 0.0699 |
| $R_p$ | | 0.0621 | 0.0404 | 0.0516 | 0.0432 |
| $\chi^2$ | | 1.19 | 2.37 | 5.39 | 5.01 |

atomic positions taken from $Sr_3Ti_2O_7$,[20] with Ln/Sr(2), Mn/Cr, O(2) and O(3) atoms situated at special positions 4e, 4e, 4e and 8g with coordinates (0, 0, *z*), (0, 0, *z*), (0, 0, z) and (0, 0.5, *z*) respectively. The Ln/Sr(1) atoms are located at (0, 0, 0.5) in sites 2b, and the O(1) atoms at (0, 0, 0) in sites 2a. The refinement values, structural parameters and *R*-factors along with the estimated standard deviation (ESD) for the phases are given in the Table 1.

The results suggest that the occupancy of oxygen in $La_{0.8}Ln_{0.2}Sr_2MnCrO_7$ phases at the site (0, 0, 0) is less than one, which shows that the phases are oxygen deficient with composition $La_{0.8}Ln_{0.2}Sr_2MnCrO_{7-\delta}$. It may be noted that of the three oxygen positions, the O(1) site is of course, the preferred one for the oxygen loss in these type of phases.[21] The decrease in oxygen content suggest that manganese is present in mixed valence state of $Mn^{3+}/Mn^{4+}$. The temperature factor ($U_{iso}$) has comparatively large values for various ions, especially the oxygen ions, signifying distortion of the ions from their ideal positions. The reliable parameters $R_{wp}$, $R_p$ and $\chi^2$ (Table 1) for the phases are reasonable for assigning the structure to the phases on the basis of the Rietveld analysis. The observed, calculated, and difference profile for the Rietveld refinement of $LaSr_2MnCrO_{7-\delta}$ phase is shown in Figure 2, while its unit cell structure is shown in Figure 3. The Rietveld refinement profiles of the other phases are shown in Figures S1, S2 and S3 in supporting information.

The data in Table 1 suggest that both the unit cell parameters *a* and *c* and cell volume decreases from La to Dy compound which is consistent with the decrease in the ionic radii of lanthanide ion. It has been observed that the decrease

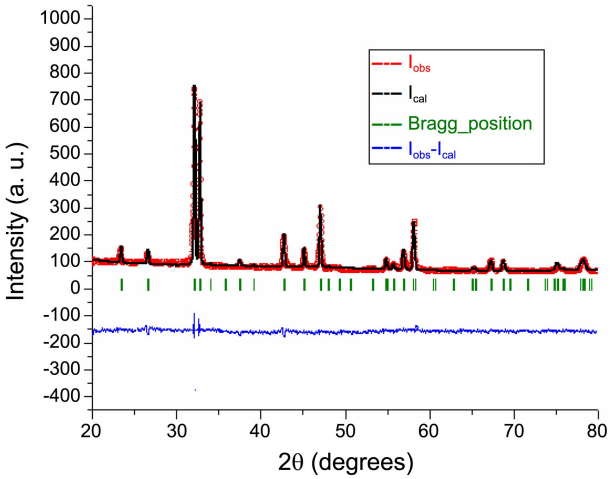


**Figure 2.** Rietveld refinement profile for the fit to the XRD pattern of $LaSr_2MnCrO_7$.

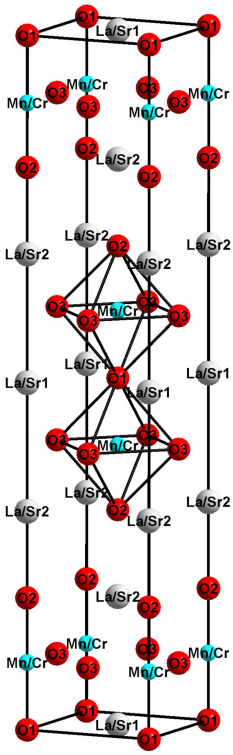


**Figure 3.** Unit cell structure of $LaSr_2MnCrO_7$.

in *c* parameter from La to Dy is much larger than that of *a* parameter. This can be attributed to the commulative effect of reduced lanthanide radii along the *c* direction where the layers are stacked. The particle size (*D*) was determined from XRD using the Scherrer equation[22]

$$D = \frac{K\lambda}{\beta \cos\theta}$$

where *K* is a constant equal to 0.90, $\lambda$ is the incident X-ray wavelength (= 1.54 Å), $\theta$ is diffraction angle and $\beta$ is full width of the peak at half maximum in radians. The particle sizes, as determined from peak with maximum intensity which corresponded to the Miller indices (105) in all XRD patterns, are given in Table 2. The change in particle size was attributed to the ionic radii of the constituent lanthanide ion. The crystallites were more compact in the sample $La_{0.8}Dy_{0.2}Sr_2MnCrO_7$ as $Dy^{3+}$ ion was smallest one. Substitution of lanthanide ion with larger ionic radius caused an increase in porosity of grains and the grains were less compact causing an increase in particle size.

**Table 2.** Particle size, density and percentage porosity of $La_{0.8}Ln_{0.2}Sr_2MnCrO_7$ phases

| Compound | Particle size (nm) | Experimental density (g cm$^{-3}$) | X-ray density (g cm$^{-3}$) | %age Porosity |
|---|---|---|---|---|
| $LaSr_2MnCrO_7$ | 40.54 | 5.576 | 5.947 | 6.24 |
| $La_{0.8}Nd_{0.2}Sr_2MnCrO_7$ | 38.35 | 5.657 | 5.992 | 5.59 |
| $La_{0.8}Gd_{0.2}Sr_2MnCrO_7$ | 36.30 | 5.773 | 6.047 | 4.53 |
| $La_{0.8}Dy_{0.2}Sr_2MnCrO_7$ | 35.31 | 5.851 | 6.075 | 3.69 |

The temperature dependence of inverse molar magnetic susceptibility is shown in Figure 4. The linearity of plots suggests that the Curie-Weiss law is followed in the temperature region of investigation. The values of magnetic moment ($\mu_{eff}$), estimated from high temperature region of $\chi_m^{-1}$ *versus* T plot (Fig. 4), are given in the Table 3. The theoretical spin only magnetic moments for the phases have been calculated from the relationship[23]

$$\mu_{cal} = \sqrt{n_1\mu_1^2 + n_2\mu_2^2 + n_3\mu_3^2}$$

where $n_1$, $n_2$ and $n_3$ are the relative molar fractions of $Ln^{3+}$, $Mn^{4+}$ and $Cr^{3+}$ ions, while $\mu_1$, $\mu_2$ and $\mu_3$ are their respective theoretical magnetic moments and are given in Table 3. The higher values of $\mu_{eff}$ than $\mu_{cal}$ show that manganese is partly present in +3 valence state. The difference in the values of $\mu_{eff}$ and $\mu_{cal}$ suggest that the phases contain about 20% $Mn^{3+}$ and 80% $Mn^{4+}$, which is in good agreement with the occupancy of oxygen determined by Rietveld analysis. The

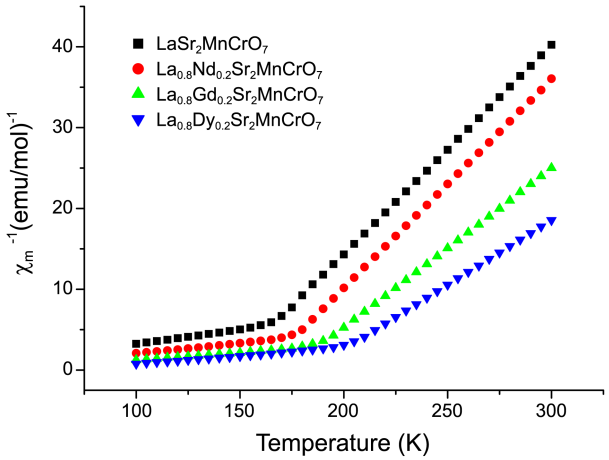


**Figure 4.** Plots of inverse molar magnetic susceptibility ($\chi_m^{-1}$) *versus* Temperature (K) of $LaSr_2MnCrO_7$, $La_{0.8}Nd_{0.2}Sr_2MnCrO_7$, $La_{0.8}Gd_{0.2}Sr_2MnCrO_7$, and $La_{0.8}Dy_{0.2}Sr_2MnCrO_7$.

**Table 3.** Magnetic and electrical parameters of $La_{0.8}Ln_{0.2}Sr_2MnCrO_7$ giving the values of Weiss constant (θ), Curie temperature ($T_C$), Curie constant (C), theoretical magnetic moment of rare-earth ion ($\mu_{Ln^{3+}}$), experimental magnetic moment ($\mu_{eff}$), calculated spin-only magnetic moment ($\mu_{cal}$), and characteristic VRH temperature ($T_o$)

| Compound | θ (K) | $T_C$ (K) | C (Kemu/mol) | $\mu_{Ln^{3+}}$ (B. M.) | $\mu_{eff}$ (B. M.) | $\mu_{cal}$ (B. M.) | $T_o \times 10^{-6}$ (K) |
|---|---|---|---|---|---|---|---|
| $LaSr_2MnCrO_7$ | 144 | 165 | 3.963 | 0.0 | 5.63 | 5.48 | 6.797 |
| $La_{0.8}Nd_{0.2}Sr_2MnCrO_7$ | 152 | 170 | 4.323 | 3.62 | 5.88 | 5.71 | 5.186 |
| $La_{0.8}Gd_{0.2}Sr_2MnCrO_7$ | 165 | 185 | 5.563 | 7.94 | 6.67 | 6.53 | 3.820 |
| $La_{0.8}Dy_{0.2}Sr_2MnCrO_7$ | 180 | 200 | 6.828 | 10.63 | 7.39 | 7.25 | 2.575 |

Weiss constant (θ) is positive for all the phases suggesting that the ferromagnetic interactions are dominant. Similar results were also reported by Zhang et al for the doping of Cr in bilayered $LaSr_2Mn_2O_7$.[11] The ferromagnetic Curie temperature ($T_C$) for the phases was determined from the plot of molar magnetic susceptibility ($\chi_m$) *versus* temperature (see supporting information Fig. S4) as well as from the plot of product of molar magnetic susceptibility and temperature ($\chi_m T$) *versus* temperature (see supporting information Fig. S5) and its values are given in Table 3.

The magnetic properties of the manganites are determined by the sum of contributions from several exchange interaction mechanisms, more specifically, superexchange interaction of manganese ions *via* oxygen ions, double exchange in the presence of manganese ions in different valence states, and indirect exchange *via* free carriers. The last two mechanisms are qualitatively similar and account for the ferromagnetic coupling between the magnetic ions. Since in the present phases, Mn is present in mixed valence state ($Mn^{3+}$/$Mn^{4+}$), there could be ferromagnetic DE interaction between $Mn^{3+}$ and $Mn^{4+}$ ions. Moreover, the $Cr^{3+}$ ion has the same electronic configuration ($t_{2g}^3 e_g^o$) as the $Mn^{4+}$ ion, there may exist a ferromagnetic DE interaction between $Cr^{3+}$ and $Mn^{3+}$ ions just as between $Mn^{4+}$ and $Mn^{3+}$ ions. The proposal has been proved by some experimental results.[24] Thus, the double exchange couplings $Mn^{3+}$–O–$Mn^{4+}$ and $Mn^{3+}$–O–$Cr^{3+}$ leads to ferromagnetic interactions in these phases. Both Weiss constant (θ) and ferromagnetic Curie temperature ($T_C$) increases with decrease in the ionic radius of lanthanide ion (Table 3). $Ln^{3+}$ (Ln = Nd, Gd, and Dy) ions will interact with Mn/Cr ions and influence the alignment of Mn/Cr moments, which could result in the weakening of FM interaction and the frustration of long-range magnetic ordering. These effects are negligible at low doping level and long-range FM ordering is still strong.[25] Moreover, in these phases, which are quasi two-dimensional in structure, decrease in *c*-axis brings the bilayers closer thereby strengthen the coupling between them and result in the increase of three-dimensional magnetic ordering and formation of FM clusters. This seems to be the reason for increase in θ and $T_C$ for the phase with smaller unit cell.[26]

For electrical resistivity measurements, a very dense ceramic is required. The powders were fabricated into pellets (10 mm in diameter and 1 mm thick) using uniaxial pressing (20 MPa), and then sintered at 1200 °C in static air atmosphere in an electric tube furnace for about 12 h. The experimental densities of the sintered pellets were about 95% of the theoretical density. The percentage porosity of the samples was calculated using the relation.[27]

$$\rho = \left[1 - \left(\frac{d_{mea}}{d_{cal}}\right)\right] \times 100$$

where $d_{mea}$ is the measured density and $d_{cal}$ is the X-ray density. The measured density of the sintered pellets, X-ray density and the percentage porosity are given in Table 2.

The temperature dependence of electrical resistivity of $La_{0.8}Ln_{0.2}Sr_2MnCrO_{7-\delta}$ phases is illustrated in Figure 5, where log ρ is plotted against temperature (T). The plot shows that the temperature coefficient of resistivity of all the phases is negative suggesting that the materials are insulators with no anomalous features in the entire temperature range of 150-350 K. The insulating behavior arises from localization of charge carriers. It has been observed that the electrical resistivity of the phases decreases with decreasing ionic radius of lanthanide ion. This could be attributed to enhancement of three-dimensional magnetic ordering because of coming closer of $(Mn/Cr)O_2$ and (Ln,Sr)O layers along the *c*-axis as a result of the decrease in the ionic radii of lanthanide ions.[26]

The temperature dependent resistivity can be best fitted with the Mott's variable range hopping (VRH) model, $\rho = \rho_o \exp(T_o/T)^{1/4}$, where $\rho_o$ is the pre-exponential factor and $T_o$ is the characteristic VRH temperature which is proportional to Mott localization energy. $T_o$ is related to localization length

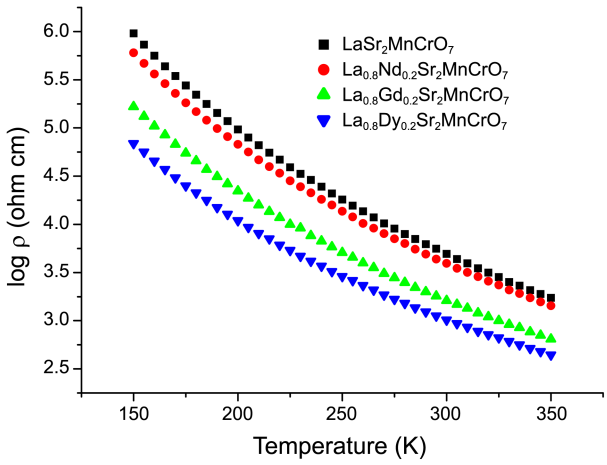


**Figure 5.** Plots of log ρ *versus* Temperature (K) of $LaSr_2MnCrO_7$, $La_{0.8}Nd_{0.2}Sr_2MnCrO_7$, $La_{0.8}Gd_{0.2}Sr_2MnCrO_7$, and $La_{0.8}Dy_{0.2}Sr_2MnCrO_7$.

($\xi$) by the relation, $T_o = 24/\pi k_B N(E_F)\xi^3$, where $k_B$ is Boltzmann constant and $N(E_F)$ is the density of states at Fermi level. The linearity of log ρ *versus* $T^{-1/4}$ plot (see supporting information Fig. S6) in the temperature range of investigation shows that the electronic conduction occurs by a 3D variable range hopping (VRH) mechanism, which is generally observed in such perovskite-related phases.[11,13] The values of $T_o$, calculated from the slopes of plots of log ρ *versus* $T^{-1/4}$, are given in Table 3. The values of $T_o$ increase with increasing size of lanthanide ion thereby increasing Mott localization energy and thus makes the transport behavior more and more insulating.

## Conclusions

Ruddlesden-Popper phases, $La_{0.8}Ln_{0.2}Sr_2MnCrO_{7-\delta}$ with Ln = La, Nd, Gd, and Dy, were synthesized by sol-gel method. The Rietveld refinement of the powder X-ray diffraction data shows tetragonal symmetry with space group *I4/mmm* for all the phases. Both the cell parameters *a* and *c* decrease from La to Dy, consistent with the decrease in the ionic radii of lanthanide ion. The phases are oxygen deficient indicating the presence of mixed valence state of manganese ($Mn^{3+}/Mn^{4+}$). The resistivity measurements suggests that the phases are insulators and the electrical conduction in the phases occurs by Mott's variable range hopping mechanism. The polycrystalline materials are ferromagnetic due to double exchange coupling between $Mn^{3+}$–O–$Mn^{4+}$ and $Mn^{3+}$–O–$Cr^{3+}$. The increase in θ and $T_C$ with decreasing ionic radius of lanthanide ion could be due to enhancement of the three-dimensional magnetic ordering because of coming closer of $(Mn/Cr)O_2$ and (Ln,Sr)O layers along the *c*-axis as a result of the decrease in the ionic radii of lanthanide ions.

**Acknowledgments.** Authors are thankful to University Grants Commission, New Delhi for financial support. Thanks are also due to Prof. Ramesh Chandra, Institute Instrumentation Centre, Indian Institute of Technology, Roorkee, for recording XRD data. And the publication cost of this paper was supported by the Korean Chemical Society.

## References

1. Moritomo, Y.; Asamitsu, A.; Kuwahara, H.; Tokura, Y.; Matsui, Y. *Nature (London)* **1996**, *380*, 141.
2. Kimura, T.; Tomioka, Y.; Kuwahara, H.; Asamitsu, A.; Tamura, M.; Tokura, Y. *Science* **1996**, *274*, 1698.
3. Kimura, T.; Tokura, Y. *Annu. Rev. Mater. Sci.* **2000**, *30*, 451.
4. Zener, C. *Phys. Rev.* **1951**, *82*, 403.
5. de Gennes, P. G. *Phys. Rev.* **1960**, *118*, 141.
6. Goodenough, J. B. *Phys. Rev.* **1955**, *100*, 564.
7. Millis, A. J.; Littlewood, P. B.; Shraiman, B. I. *Phys. Rev. Lett.* **1995**, *74*, 5144.
8. Maignan, A.; Damay, F.; Barnabe, A.; Martin, C.; Hervieu, M.; Raveau, B. *Philos. Trans. R. Soc. London Ser. B* **1998**, *356*, 1635.
9. Raveau, B.; Maignan, A.; Martin, C. *J. Solid State Chem.* **1997**, *130*, 162.
10. Barnabe, A.; Maignan, A.; Hervieu, M.; Damay, F.; Martin, C.; Raveau, B. *App. Phys. Lett.* **1997**, *71*, 3907.
11. Zhang, R. L.; Zhao, B. C.; Song, W. H.; Ma, Y. Q.; Yang, J.; Sheng, Z. G.; Dai, J. M. *J. Appl. Phys.* **2004**, *96*, 4965.
12. Yu, G.; Xu, B.; Xiong, J.; Liu, X.; Liu, L.; Yuan, S. *J. Mag. Mag. Mat.* **2011**, *323*, 1925.
13. Singh, D.; Singh, R. *J. Chem. Sci.* **2010**, *122*, 807.
14. Mahesh, R.; Mahendiran, R.; Raychaudhuri, A. K.; Rao, C. N. R. *J. Solid State Chem.* **1995**, *114*, 297.
15. Hwang, H. Y.; Cheong, S. W.; Radaelli, P. G.; Marezio, M.; Batlogg, B. *Phy. Rev. Lett.* **1995**, *75*, 914.
16. Maignan, A.; Simon, C.; Caignaert, V.; Raveau, B. *Solid State Comm.* **1995**, *96*, 623.
17. Dhahri, A.; Dhahri, J.; Dhahri, E. *J. Alloys Compds.* **2010**, *489*, 9.
18. Mazaheri, M.; Akhavan, M. *J. Mag. Mag. Mat.* **2010**, *322*, 3255.
19. Larson, A. C.; Von Dreele, R. B. *General Structure Analysis System (GSAS)*, *Los Alamos National Laboratory Report LAUR* **2004**, 86-748.
20. Ruddlesden, S. N.; Popper, P. *Acta Cryst.* **1958**, *11*, 54.
21. Dann, S. E.; Weller, M. T.; Curie, D. B. *J. Solid State Chem.* **1992**, *97*, 179.
22. Klung, H. P.; Alexander, L. E. *X-ray Diffraction Procedures: For Polycrystalline and Amorphous Materials*; John Wiley and Sons Inc.: Canada, 1954.
23. Taguchi, H. *J. Solid State Chem.* **1997**, *131*, 108.
24. Maignan, A.; Martin, C.; Damay, F.; Hervien, M.; Raveau, B. *J. Magn. Magn. Mat.* **1998**, *188*, 185.
25. Zhang, J.; Wang, F.; Zhang, P.; Yan, Q. *J. Phys.: Condens. Matter* **1999**, *11*, 2413.
26. Sharma, I. B.; Singh, D.; Magotra, S. K. *J. Alloys Compds.* **1998**, *269*, 13.
27. Cullity, B. D. *Elements of X-ray diffraction Reading*, 2nd ed.; Addision-Wesley Publishing Co.